Monolayer-to-Mesoscale Modulation of the Optical Properties in 2D CrI_3 Mapped by Hyperspectral Microscopy

Marta Galbiati,[1,*,‖] Fernando Ramiro-Manzano,[1,2,†,‖] José Joaquín Pérez Grau,[1] Fernando Cantos-Prieto,[1] Jaume Meseguer-Sánchez,[1] Ivona Kosic,[1] Filippo Mione,[1] Ana Pallarés Vilar,[1] Andrés Cantarero,[1] David Soriano,[3,4] and Efrén Navarro-Moratalla[1,‡]

[1]*Instituto de Ciencia Molecular, Universitat de València, Calle Catedrático José Beltrán Martínez 2, 46980, Paterna, Spain*
[2]*Instituto de Tecnología Química, Universitat Politècnica de València—Consejo Superior de Investigaciones Científicas (UPV-CSIC), Avd. de los Naranjos s/n, 46022, Valencia, Spain*
[3]*Information Engineering Department, University of Pisa, Via Caruso 16, 56122, Pisa, Italy*
[4]*Departamento de Física Aplicada, Universidad de Alicante, 03690, San Vicente del Raspeig, Alicante, Spain*

(Received 12 September 2022; accepted 13 March 2023; published 27 April 2023)

Magnetic 2D materials hold promise to change the miniaturization paradigm of unidirectional photonic components. However, the integration of these materials in devices hinges on the accurate determination of the optical properties down to the monolayer limit, which is still missing. By using hyperspectral wide-field imaging at room temperature, we reveal a nonmonotonic thickness dependence of the complex optical dielectric function in the archetypal magnetic 2D material CrI_3 extending across different length scales: onsetting at the mesoscale, peaking at the nanoscale, and decreasing again down to the single layer. These results portray a modification of the electronic properties of the material and align with the layer-dependent magnetism in CrI_3, shedding light on the long-standing structural conundrum in this material. The unique modulation of the complex dielectric function from the monolayer up to more than 100 layers will be instrumental for understanding mesoscopic effects in layered materials and tuning light-matter interactions in magnetic 2D materials.

DOI: 10.1103/PhysRevLett.130.176901

The dependence of the physical properties of van der Waals materials with the number of layers has been the flagship of two-dimensional (2D) materials since their discovery. In general, this layer dependence gains importance upon approaching the single layer limit, where the strict confinement of electrons in a 2D lattice imposes dramatic changes in the electronic structure of the crystal, enabling the realization of new electronic states and quantum correlated phases of matter [1–7]. Beyond the single layer limit, the properties of van der Waals materials change gradually until reaching the bulk properties generally within the nanoscale thickness. A much more unusual case features a continuous change of the material properties at much larger thicknesses. One of the few examples is the effect of layer number on the photoluminescence of hexagonal boron nitride [8]. However, this phenomenon arises from a variation of the band gap and activation energies of impurities in the system and is not a consequence of the layer dependence of the intrinsic electronic properties. Another remarkable case is chromium triiodide (CrI_3), one of the first layered materials to exhibit net magnetization down to the monolayer [9], accompanied by a transition from layered antiferromagnetic in the few-layer regime to ferromagnetic in the bulk, with a crossover thickness that is still unclear but unambiguously located in the tens of nanometers range [10–12]. Seminal studies attribute this change to differences in the stacking between the layers [13] being the ferromagnetic and layered antiferromagnetic states related to the rhombohedral and monoclinic stacking, respectively [14,15]. This points to a profound layer-dependent effect at the mesoscale, setting an imperious need to study the evolution of the electronic properties as a function of the layer count to understand the underlying mechanisms giving rise to the magnetism in CrI_3.

An insightful and nondestructive way to study the layer-dependent evolution of the electronic properties of a layered material is to determine the complex dielectric function via light-matter interaction. Although optical ellipsometry is usually employed to extract these parameters from thin films, the small sample footprints of most mechanically exfoliated 2D materials hinder the direct application of this technique. One strategy to overcome the spatial resolution limitation is to use an optical microscope equipped with a broadband white light source coupled to a spectrometer, where a continuous adjustment of the illumination wavelength in constrained areas of the sample allows for an accurate extraction of the dielectric function in the visible range [16]. However, the sampling speed and data statistics of point spectroscopy are generally low. Wide-field hyperspectral microscopy on the other hand has been successfully employed for the high-throughput

layer-dependent characterization of 2D materials and heterostructures in air [17–20]. Unfortunately, the magnetic 2D materials are very sensitive to the presence of humidity and oxygen and therefore require an appropriate isolation from ambient conditions and rapid characterization to preclude the effect of degradation, a combination of requirements that until now has not been met by the established protocols. By developing a simple encapsulation technique compatible with wide-field hyperspectral imaging, we herein circumvent the low throughput of deterministic encapsulation and achieve high sampling and data reliability in the characterization of the layer-dependent optical properties of CrI_3. The use of a monochrome camera with a high linear dynamic range permits a single-shot acquisition of the light intensity coming from tens of CrI_3 crystals with different thickness, providing simultaneous access to large statistics while minimizing the acquisition times. By then modeling the spectral information obtained as a function of the layer number, we identify two crossover points of the complex optical dielectric function of CrI_3, one at the nanoscale and one at the mesoscale range of thickness. Our theoretical results based on first-principles calculations provide support to the electronic origin of the evolution of the dielectric function with the layer number. Remarkably, the modulation of the optical properties with a crossover to the bulk regime at the mesoscale is a physical phenomenon not previously reported for van der Waals materials and casts light on deep open questions regarding magnetic 2D materials, such as the striking stacking order differences between thick multilayer and bulk CrI_3 [13,21] and the resulting magnetic ground states of the mesoscopic multilayers [11,12,22,23].

We obtained CrI_3 flakes from the single layer to the hundreds-of-layers thickness range by mechanical exfoliation of bulk crystals on standard microscopy glass slides. All the flakes were atomically flat and chemically pristine as confirmed by atomic force microscopy (AFM; see Supplemental Material [24] Sec. 1.4 for details) and Raman spectroscopy [Fig. 1(b); see Supplemental Material [24] Sec. 1.3 for details]. The samples were then encapsulated with a coverslip sealed using a thermoplastic material to avoid degradation. Spatially resolved hyperspectral maps of different regions of the sample were then acquired at room temperature by combining a sequence of optical images recorded under monochromatic illumination spanning the full visible range (see Supplemental Material [24] Sec. 2).

After considering different approaches for the evaluation of the complex dielectric function from optical data (see Supplemental Material [24] Sec. 3), we chose to focus on transmission measurements with large statistics to achieve high data reliability. By analyzing the hyperspectral transmission maps in selected regions of CrI_3 crystals of homogeneous thickness, we obtained spectral traces of

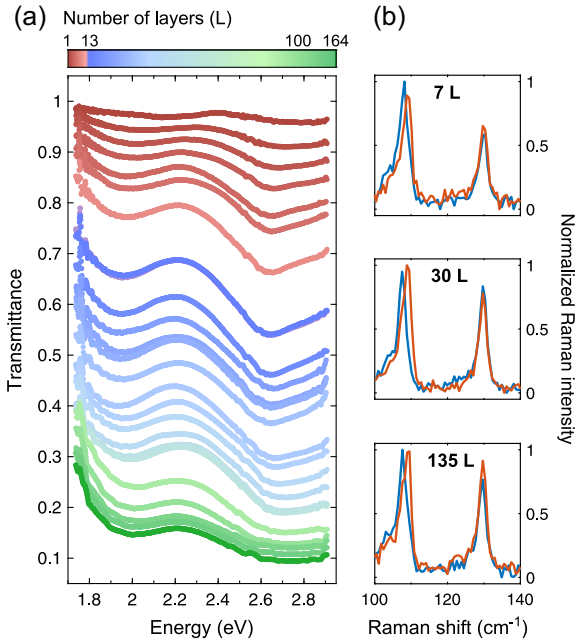

FIG. 1. Spectroscopic characterization of CrI_3. (a) Visible range transmittance spectra of CrI_3 crystals with a different number of layers. Red curves correspond to thin layers (from 1 to 13 L), blue curves to layers ranging from 14 to ~100 L, and green curves correspond to bulk (up to 164 L). (b) Polarized Raman scattering of CrI_3 crystals with thicknesses in the few-layer (7 L), multilayer (30 L), and bulk (135 L) ranges. Red and blue curves have been taken with a 45° shift in the polarization angle with respect to the crystallographic axis. The small spectral shift of about 2 cm^{-1} confirms that the stacking order is monoclinic.

the material for different layer numbers. Figure 1(a) shows a representative set of transmittance spectra of flakes with a thickness ranging from 1 layer (L) to 164 L. Two absorption features are visible at about 1.95 and 2.7 eV corresponding to the ligand-to-metal charge transfer absorption peaks reported for bulk CrI_3 and more recently for CrI_3 exfoliated samples [31–33]. Remarkably, both transmittance dips present a nonmonotonic trend with the number of layers, i.e. a redshift when flake thickness increases from 1 to ~13 L, a blueshift above ~50 L, and a smooth crossover toward the bulk spanning the mesoscopic scale up to ~100 L, the point beyond which these features remain almost unchanged. This suggests a change in the optical properties of CrI_3 with marked thickness regimes both at the nanoscale and the mesoscale.

To extract the complex dielectric function ($\tilde{\varepsilon} = \varepsilon_1 - i\varepsilon_2$) of CrI_3 from the transmittance data and limit the interdependence and ranges of ε_1 and ε_2, we simultaneously analyzed transmittance spectra acquired over flakes with different thicknesses from different samples with ample statistics (thousands of pixels for each layer number). We consider our experimental system as a basic Fabry-Pérot cavity formed by a stack of three layers, and we assume that

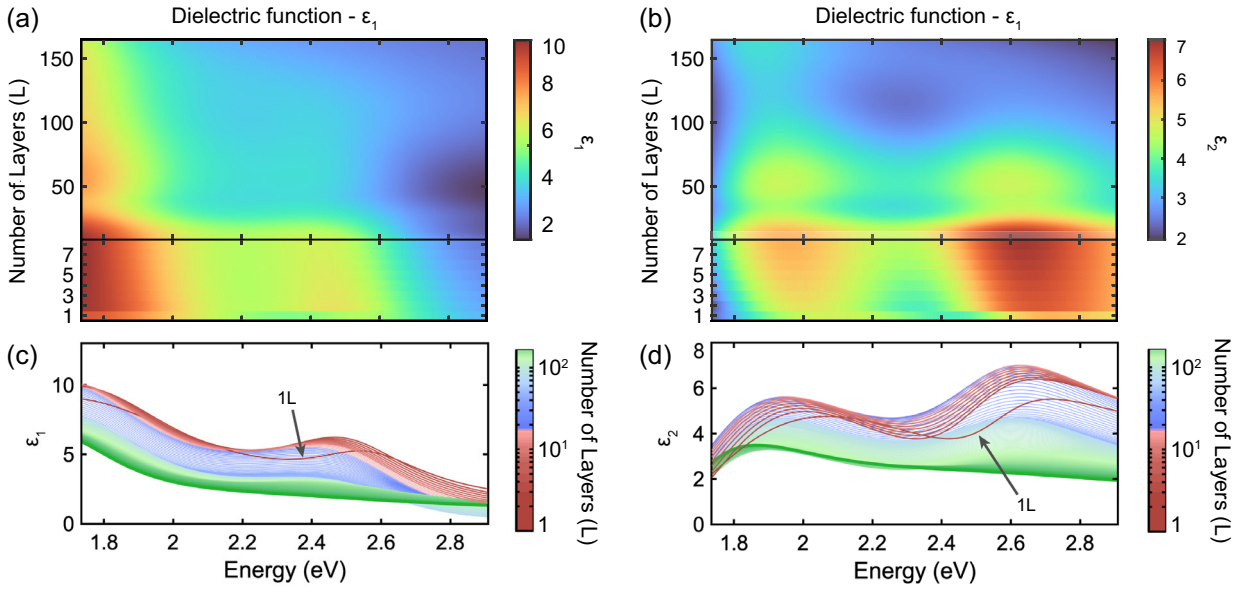

FIG. 2. Evolution of the dielectric functions in CrI_3 as a function of the layer number. The calculated real (ε_1) and imaginary (ε_2) parts of $\tilde{\varepsilon}$ are represented by color maps [(a),(b)] and line plots [(c),(d)], respectively.

the dielectric function of CrI_3 follows a modified Lorentzian oscillator model [34]:

$$\tilde{\varepsilon}(\omega) = \varepsilon_\infty + \sum_{n=1}^{2} \frac{\omega_{p_n}^2 + 2i\omega\Gamma_n}{\omega_{0_n}^2 - \omega^2 + 2i\omega\gamma_n}.$$

This model is composed by two oscillators ($n = 1, 2$), where ε_∞ is the permittivity for infinite optical frequencies, ω_{0_n}, ω_{p_n}, and ω represent the resonant, plasma, and photon frequency, respectively, and γ_n and Γ_n are damping-related parameters. Figure 2 shows the real and imaginary parts of $\tilde{\varepsilon}(\omega)$ and their evolution with flake thickness calculated by simultaneous fitting of all the transmittance spectra shown in Fig. 1 (see Supplemental Material [24] Sec. 3). An initial inspection of the dielectric traces reveals that the dielectric function of the CrI_3 monolayer is significantly different from the rest of the layers. This is in line with the transmittance spectra experimentally measured in the monolayer, where absorption features are significantly shifted compared to the bilayer. In addition, we find two additional crossover points at ~13 L (~9.1 nm) and ~100 L (~69.8 nm), where the ε_2 intensity increases and peaks redshift (<13 L), then decreases and peaks blueshift (>13 L), until it starts to asymptotically saturate

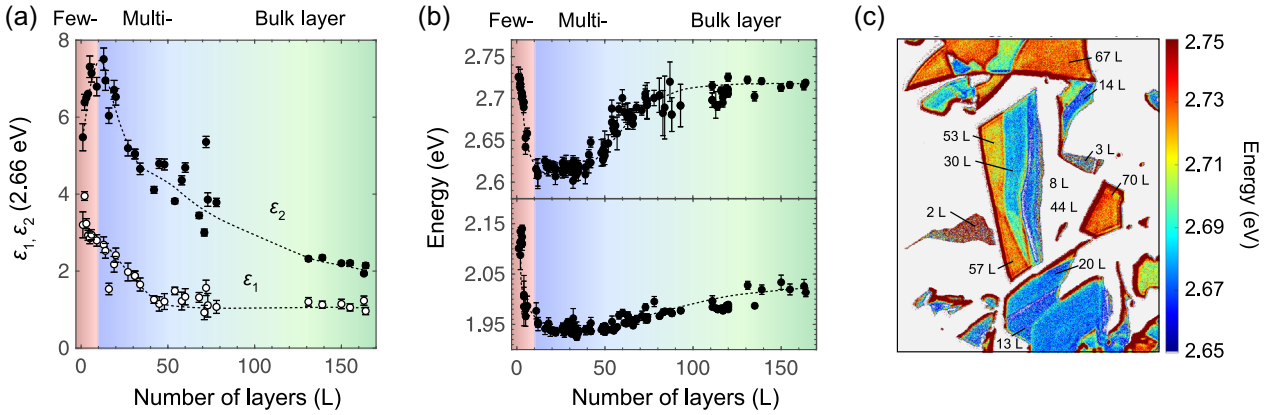

FIG. 3. Identification of different thickness regimes in CrI_3. The few-layer, multilayer, and bulk thickness regimes are depicted according to (a) the layer dependence of ε_1 and ε_2 at 2.66 eV from the fitting process to the dataset shown in Fig. 1; (b) the low- (bottom) and high- (top) energy transmittance minima experimentally measured in the spectra of the dataset shown in Fig. 1, and additional ones, demonstrating the good reproducibility of the results (see Supplemental Material [24] Sec. 2.3). Dotted lines are guides to the eye. (c) Spatially resolved wide-field image of the high-energy transmittance dip position calculated from hyperspectral images of CrI_3 flakes.

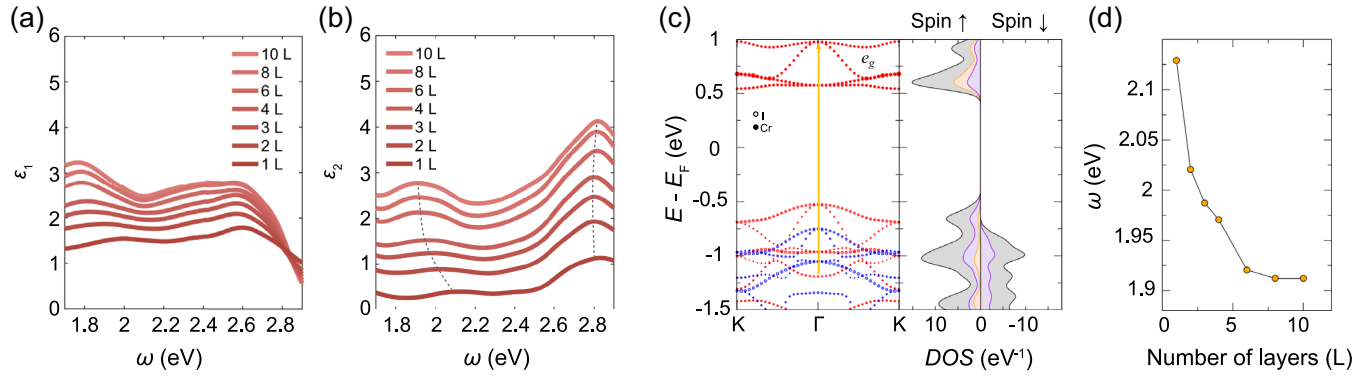

FIG. 4. Theory calculations of the layer-dependent electronic and optical properties of CrI_3. (a),(b) Evolution of ε_1 and ε_2 of CrI_3 with an increasing number of layers calculated in the z direction perpendicular to the layers. (c) Projected band structure and DOS of monolayer CrI_3. Filled and empty circles represent I p orbitals and Cr d orbitals, respectively. The size of the circles is the weight of the orbital wave function in each band. Red and blue stand for spin up and down, respectively. The yellow arrow shows the most probable transition responsible for the low-energy peak in the dielectric function. (d) Evolution of the low-energy peak of ε_2 with an increasing number of layers.

toward the bulk value above ~100 L. This delimits three different thickness domains: (i) few layer, (ii) multilayer, and (iii) bulk.

These changes are also clearly illustrated in Fig. 3 which shows the evolution with layer thickness of ε_1 and ε_2 at 2.66 eV extracted from the fitting process [Fig. 3(a); see Supplemental Material [24] Sec. 3.2], and the evolution of the experimental absorption minima of the transmittance spectra [Fig. 3(b); see Supplemental Material [24] Sec. 3.4]. The small uncertainty and good consistency of both fitting process and experimental results [Figs. 3(a) and 3(b)] provide evidence of the robustness of our analysis. Finally, hyperspectral analysis also gives the possibility to spatially resolve the optical properties of the 2D material. As such, Fig. 3(c) displays the spatially resolved wide-field image of the higher-energy transmittance dip of CrI_3 flakes for different thicknesses (see Supplemental Material [24] Sec. 4) where the energy crossover of the dip position from few-layer (red to blue palette) to bulk (blue to red palette) is also clearly visible. These experimental observations point at profound changes in the optical properties of CrI_3 in these three different thickness regimes.

The evolution of $\tilde{\varepsilon}$ with the layer number has been previously reported in other 2D materials such as transition metal dichalcogenides (TMDCs) [35], In_2Se_3 [36], $PdSe_2$ [37], and a nonmonotonic behavior was observed in MoS_2 at the nanoscale [38]. However, in all of these cases, this behavior has been reported only in the nanoscale, while this is the first time that a modulation of $\tilde{\varepsilon}$ has been experimentally observed at the mesoscale range of thickness, allowing for a continuous modulation of the optical properties from one to more than 100 layers.

A possible origin of the nonmonotonic variation of the optical properties with the number of layers could be a change of the atomic structure of the crystal. To preclude the existence of layer-dependent stacking order at room temperature, we performed polarized Raman scattering of flakes covering the entire thickness range of our dataset (see Supplemental Material [24] Sec. 1.3). Typical changes in the crystal structure of these compounds are produced by alterations of the stacking order of the layers, which results in modifications of the point group of the structure and the Raman tensors [39,40], resulting in the splitting of different vibrations modes. Figure 1(b) portrays representative examples of the three low-Raman-shift modes that can be ascribed to the monoclinic phase of CrI_3 (C_{2h}). As the angular dependence of the intensity of the modes is insensitive to the layer number in the full range of our samples, we can discard the stacking effect as the origin of the optical properties modulation observed.

To gain insight into alternative origins of the layer dependence of the optical properties, we carried out first-principles calculations on few-layer CrI_3, up to 10 L (see Supplemental Material [24] Sec. 5). At room temperature, long-range magnetic ordering is lost and CrI_3 becomes paramagnetic. In the absence of spin interactions, density functional theory (DFT) calculations fail to reproduce the band gap of CrI_3 and give rise to a metallic phase [41]. For this reason, our calculations are carried out in the antiferromagnetic monoclinic phase. This does not dramatically affect our results, since the most active optical transitions are spin conserved, and the crystal-field splitting is weakly affected by the temperature. Moreover, previous works demonstrate that the electronic structure of the material is barely modified by the absence of magnetic order [14,42,43], underpinning the qualitative validity of the theoretical layer-dependence trends at room temperature. In the imaginary part of the computed dielectric function [Figs. 4(a) and 4(b)], we identify two peaks located at 2.1 and 2.8 eV, qualitatively in good agreement with the experimental results. A look at the band structure and

DOS of monolayer CrI_3 [Fig. 4(c)] confirms that these peaks can be ascribed to metal-to-ligand charge transfer processes between the p orbitals of the ligands, localized in the last occupied bands, and the empty $d_{x2\text{-}y2}$ and d_{z2} orbitals of the chromium atoms localized in the e_g set of conduction bands. In Fig. 4(d), we plot the evolution of the peak at 2.1 eV with an increasing number of layers. We observe a strong redshift from 2.1 to 1.9 eV and a stabilization of the shift at around ten layers in agreement with the experimental data, indicating a clear connection between the electronic structure and the layer dependence and crossover point of the optical properties at the nanoscale.

The calculations also show how the value of the complex dielectric function increases when increasing the thickness from 1 to 10 L, in agreement with the experiments. The discrepancies in the absolute value of the complex dielectric functions extracted from the calculations and the experiments may originate from subtle differences of the interlayer distance and the temperature [44]. To shed some light on this point, we have carried out a series of dielectric function calculations for increasing values of the interlayer distance in bilayer CrI_3 (see Supplemental Material [24] Sec. 5). Our calculations clearly indicate that the intensity of the complex dielectric function decays for larger interlayer distances. These results suggest that small changes in the interlayer distance when going from few-layer to bulk CrI_3 could eventually modify the intensity of the complex dielectric function. Indeed, the average interlayer distance in bulk antiferromagnetic CrI_3 obtained from DFT calculations is 0.2 Å higher than in few-layer samples (see Supplemental Material [24] Table S2). Although these results are not able to explain the crossover at the nanoscale regime, they highlight the importance of van der Waals interactions in modulating the interlayer distance and the electronic properties at different thickness regimes and corroborate the experimentally observed tendency toward lower dielectric function intensities in thicker samples.

Remarkably, the unexpected crossover of the optical properties of CrI_3 at the mesoscale appears to be aligned with the critical crystal thickness at which the low-temperature magnetic properties of CrI_3 change from antiferromagnetic to ferromagnetic [9]. Although this critical thickness has not yet been unambiguously determined, most works report on the layered antiferromagnetic state persisting in crystals up to several tens of nanometers [22,23]. Both the magnetic and the optical crossover thickness to the bulk regime being in the same range might be an indication of the common origin of these phenomena. Supported by our theory calculations, we postulate that this origin is electronic in nature, although an unambiguous relationship between both phenomena occurring at different temperature ranges cannot be claimed at this stage and calls for further studies at low temperatures. Together with the crossover observed at the nanoscale thickness regime, the optical properties of CrI_3 portray a unique nontrivial layer dependence of the electronic properties of the material at room temperature. From a fundamental point of view, this is far beyond the quantum confinement layer-dependent effects reported so far, and will usher future investigations in the field of mesoscopic physics with possible observation of similar effects in other 2D materials and strong implications in the physics of the ever-growingly complex family of van der Waals heterostructures, some of which are beginning to reach the mesoscopic thickness. The significantly wide span of the continuous modulation of the optical and electronic structure with layer number, covering more than 100 layers, will also be pivotal to enable the fine-tuning of the optical properties of magnetic 2D materials and to expand the frontiers of integrated photonics.

The project that gave rise to these results received the financial support of a fellowship from the "la Caixa" Foundation (ID No. 100010434, fellowship codes LCF/BQ/PR21/11840011 and LCF/BQ/DI22/11940022) and Grant No. PID2020-118938GA-100 from the Spanish Ministerio de Ciencia e Innovación (MICINN). E. N. M. acknowledges the European Research Council (ERC) under the Horizon 2020 research and innovation program (ERC StG, Grant Agreement No. 803092). E. N. M. and M. G. acknowledge the MICINN and the European Union NextGenerationEU for financial support from the Ramon y Cajal program (Grants No. RYC2018-024736-I and No. RYC2021-034609-I). F. C. P. also acknowledges the MICINN for the FPU program (Grant No. FPU17/01587). F. R. M. acknowledges the MICINN for financial support (Grant No. PID2021-123163OB-I00). This work was also supported by the Spanish Unidad de Excelencia "María de Maeztu" (Grant No. CEX2019-000919-M) and is part of the Advanced Materials program supported by MICINN with funding from European Union NextGenerationEU (PRTR-C17.I1) and by Generalitat Valenciana. D. S. and A.C. acknowledge Generalitat Valenciana for financial support (from the CIDEGENT program Grant No. CIDEGENT/2021/052 and PROMETEO2020-016 respectively) and computational resources at University of Pisa.

*marta.galbiati@uv.es
†ferraman@fis.upv.es
‡efren.navarro@uv.es
‖These authors contributed equally to this work.

[1] K. S. Novoselov, A. K. Geim, S. V. Morozov, D. Jiang, M. I. Katsnelson, I. V. Grigorieva, S. V. Dubonos, and A. A. Firsov, Two-dimensional gas of massless Dirac fermions in graphene, Nature (London) **438**, 197 (2005).

[2] Y. Cao, V. Fatemi, S. Fang, K. Watanabe, T. Taniguchi, E. Kaxiras, and P. Jarillo-Herrero, Unconventional superconductivity in magic-angle graphene superlattices, Nature (London) **556**, 43 (2018).

[3] K. F. Mak, C. Lee, J. Hone, J. Shan, and T. F. Heinz, Atomically Thin MoS_2: A New Direct-Gap Semiconductor, Phys. Rev. Lett. **105**, 136805 (2010).

[4] A. Splendiani, L. Sun, Y. Zhang, T. Li, J. Kim, C. Y. Chim, G. Galli, and F. Wang, Emerging photoluminescence in monolayer MoS_2, Nano Lett. **10**, 1271 (2010).

[5] H. Zeng, J. Dai, W. Yao, D. Xiao, and X. Cui, Valley polarization in MoS_2 monolayers by optical pumping, Nat. Nanotechnol. **7**, 490 (2012).

[6] K. F. Mak, K. He, J. Shan, and T. F. Heinz, Control of valley polarization in monolayer MoS_2 by optical helicity, Nat. Nanotechnol. **7**, 494 (2012).

[7] X. Xi, Z. Wang, W. Zhao, J.-H. Park, K. T. Law, H. Berger, L. Forró, J. Shan, and K. F. Mak, Ising pairing in superconducting $NbSe_2$ atomic layers, Nat. Phys. **12**, 139 (2015).

[8] X. Z. Du, M. R. Uddin, J. Li, J. Y. Lin, and H. X. Jiang, Layer number dependent optical properties of multilayer hexagonal BN epilayers, Appl. Phys. Lett. **110**, 092102 (2017).

[9] B. Huang *et al.*, Layer-dependent ferromagnetism in a van der Waals crystal down to the monolayer limit, Nature (London) **546**, 270 (2017).

[10] B. Niu *et al.*, Coexistence of magnetic orders in two-dimensional magnet CrI_3, Nano Lett. **20**, 553 (2020).

[11] Z. Wang, I. Gutiérrez-Lezama, N. Ubrig, M. Kroner, M. Gibertini, T. Taniguchi, K. Watanabe, A. Imamoğlu, E. Giannini, and A. F. Morpurgo, Very large tunneling magnetoresistance in layered magnetic semiconductor CrI_3, Nat. Commun. **9**, 2516 (2018).

[12] D. R. Klein *et al.*, Probing magnetism in 2D van der Waals crystalline insulators via electron tunneling, Science **360**, 1218 (2018).

[13] Z. Sun *et al.*, Giant nonreciprocal second-harmonic generation from antiferromagnetic bilayer Very large tunneling magnetoresistance in layered magnetic semiconductor CrI_3, Nature (London) **572**, 497 (2019).

[14] M. A. McGuire, H. Dixit, V. R. Cooper, and B. C. Sales, Coupling of crystal structure and magnetism in the layered, ferromagnetic insulator Very large tunneling magnetoresistance in layered magnetic semiconductor CrI_3, Chem. Mater. **27**, 612 (2015).

[15] N. Sivadas, S. Okamoto, X. Xu, C. J. Fennie, and D. Xiao, Stacking-dependent magnetism in bilayer Very large tunneling magnetoresistance in layered magnetic semiconductor CrI_3, Nano Lett. **18**, 7658 (2018).

[16] Y. Li, A. Chernikov, X. Zhang, A. Rigosi, H. M. Hill, A. M. van der Zande, D. A. Chenet, E.-M. Shih, J. Hone, and T. F. Heinz, Measurement of the optical dielectric function of monolayer transition-metal dichalcogenides: MoS_2, $MoSe_2$, WS_2, and WSe_2, Phys. Rev. B **90**, 205422 (2014).

[17] A. Castellanos-Gomez, J. Quereda, H. P. van der Meulen, N. Agraït, and G. Rubio-Bollinger, Spatially resolved optical absorption spectroscopy of single- and few-layer MoS_2 by hyperspectral imaging, Nanotechnology **27**, 115705 (2016).

[18] R. W. Havener, C.-J. Kim, L. Brown, J. W. Kevek, J. D. Sleppy, P. L. McEuen, and J. Park, Hyperspectral imaging of structure and composition in atomically thin heterostructures, Nano Lett. **13**, 3942 (2013).

[19] Y.-C. Chang, Y.-K. Wang, Y.-T. Chen, and D.-Y. Lin, Facile and reliable thickness identification of atomically thin dichalcogenide semiconductors using hyperspectral microscopy, Nanomaterials (Basel) **10**, 526 (2020).

[20] A. Rousseau *et al.*, Monolayer boron nitride: Hyperspectral imaging in the deep ultraviolet, Nano Lett. **21**, 10133 (2021).

[21] N. Ubrig, Z. Wang, J. Teyssier, T. Taniguchi, K. Watanabe, E. Giannini, A. F. Morpurgo, and M. Gibertini, Low-temperature monoclinic layer stacking in atomically thin CrI_3 crystals, 2D Mater. **7**, 015007 (2019).

[22] Y. Liu, L. Wu, X. Tong, J. Li, J. Tao, Y. Zhu, and C. Petrovic, Thickness-dependent magnetic order in CrI_3 single crystals, Sci. Rep. **9**, 13599 (2019).

[23] T. Song *et al.*, Giant tunneling magnetoresistance in spin-filter van der Waals heterostructures, Science **360**, 1214 (2018).

[24] See Supplemental Material at http://link.aps.org/supplemental/10.1103/PhysRevLett.130.176901 for different approaches for the experimental determination of the complex dielectric function, which includes Refs. [25–27]; For extraction of the complex dielectric function from transmittance data, which includes Ref. [28]; For the calculation of the dependence of the complex dielectric function with layer number and interlayer distance, which includes Refs. [29,30].

[25] A. Castellanos-Gomez, E. Navarro-Moratalla, G. Mokry, J. Quereda, E. Pinilla-Cienfuegos, N. Agraït, H. S. J. van der Zant, E. Coronado, G. a. Steele, and G. Rubio-Bollinger, Fast and reliable identification of atomically thin layers of $TaSe_3$ crystals, Nano Res. **6**, 191 (2013).

[26] L. Tomarchio, S. Macis, L. Mosesso, L. T. Nguyen, A. Grilli, M. C. Guidi, R. J. Cava, and S. Lupi, Low energy electrodynamics of CrI_3 layered ferromagnet, Sci. Rep. **11**, 23405 (2021).

[27] H. Ibach and H. Luth, *Solid State Physics*, 2nd ed. (Springer, Berlin, 1995).

[28] P. Blake, E. W. Hill, A. H. Castro Neto, K. S. Novoselov, D. Jiang, R. Yang, T. J. Booth, and A. K. Geim, Making graphene visible, Appl. Phys. Lett. **91**, 063124 (2007).

[29] P. Giannozzi *et al.*, Advanced capabilities for materials modelling with quantum ESPRESSO, J. Phys. Condens. Matter **29**, 465901 (2017).

[30] D. Sangalli *et al.*, Many-body perturbation theory calculations using the yambo code, J. Phys. Condens. Matter **31**, 325902 (2019).

[31] P. M. Grant and G. B. Street, Optical properties of chromium trihalides in the region 1–11 EV, Bull. Am. Phys. Soc. **13**, 415 (1968).

[32] K. L. Seyler *et al.*, Ligand-field helical luminescence in a 2D ferromagnetic insulator, Nat. Phys. **14**, 277 (2017).

[33] W. Jin *et al.*, Observation of the polaronic character of excitons in a two-dimensional semiconducting magnet CrI_3, Nat. Commun. **11**, 4780 (2020).

[34] K. Prokopidis and C. Kalialakis, Physical interpretation of a modified Lorentz dielectric function for metals based on the Lorentz–Dirac force, Appl. Phys. B **117**, 25 (2014).

[35] H. Gu, B. Song, M. Fang, Y. Hong, X. Chen, H. Jiang, W. Ren, and S. Liu, Layer-dependent dielectric and optical properties of centimeter-scale 2D WSe_2: Evolution from a single layer to few layers, Nanoscale **11**, 22762 (2019).

[36] D. Wu *et al.*, Thickness-dependent dielectric constant of few-layer In_2Se_3 nanoflakes, Nano Lett. **15**, 8136 (2015).

[37] M. Wei, J. Lian, Y. Zhang, C. Wang, Y. Wang, and Z. Xu, Layer-dependent optical and dielectric properties of

centimeter-scale $PdSe_2$ films grown by chemical vapor deposition, npj 2D Mater. Appl. **6**, 1 (2022).
[38] Y. Yu *et al.*, Exciton-dominated dielectric function of atomically thin MoS_2 films, Sci. Rep. **5**, 16996 (2015).
[39] T. Li *et al.*, Pressure-controlled interlayer magnetism in atomically thin CrI_3, Nat. Mater. **18**, 1303 (2019).
[40] D. T. Larson and E. Kaxiras, Raman spectrum of CrI_3: An *ab initio* study, Phys. Rev. B **98**, 085406 (2018).
[41] D. Soriano, A. N. Rudenko, M. I. Katsnelson, and M. Rösner, Environmental screening and ligand-field effects to magnetism in CrI_3 monolayer, npj Comput. Mater. **7**, 162 (2021).
[42] J. F. Dillon and C. E. Olson, Magnetization, resonance, and optical properties of the ferromagnet CrI_3, J. Appl. Phys. **36**, 1259 (1965).
[43] X.-Y. Chen, M.-Q. Long, and Y.-P. Wang, Paramagnetic phases of two-dimensional magnetic materials, Phys. Rev. B **102**, 214417 (2020).
[44] A. J. Bosman and E. E. Havinga, Temperature dependence of dielectric constants of cubic ionic compounds, Phys. Rev. **129**, 1593 (1963).